Received: 27 December 2021 | Revised: 28 March 2022 | Accepted: 1 June 2022 | Published online: 10 July 2022

DOI: 10.1002/trc2.12325

Alzheimer's & Dementia
Translational Research & Clinical Interventions

RESEARCH ARTICLE

Measurement of neurodegeneration using a multivariate early frame amyloid PET classifier

Dawn C. Matthews[1] | **Ana S. Lukic**[1] | **Randolph D. Andrews**[1] | **Miles N. Wernick**[1] | **Stephen C. Strother**[2] | **Mark E. Schmidt**[3] | **for the Alzheimer's Disease Neuroimaging Initiative**[#]

[1]ADM Diagnostics, Inc., Northbrook, Illinois, USA

[2]Baycrest Hospital, and Department of Medical Biophysics, University of Toronto, North York, Ontario, Canada

[3]Janssen Research and Development, Division of Janssen Pharmaceutica, Beerse, Belgium

Correspondence
Dawn C. Matthews, ADM Diagnostics, Inc. 555 Skokie Blvd., Suite 500, Northbrook, IL 60062, USA.
E-mail: dmatthews@admdx.com

[#]Data used in preparation of this article were obtained from the Alzheimer's Disease Neuroimaging Initiative (ADNI) database (adni.loni.usc.edu). As such, the investigators within the ADNI contributed to the design and implementation of ADNI and/or provided data but did not participate in analysis or writing of this report. A complete listing of ADNI investigators can be found at: http://adni.loni.usc.edu/wp-content/uploads/how_to_apply/ADNI_Acknowledgement_List.pdf

Abstract

Introduction: Amyloid measurement provides important confirmation of pathology for Alzheimer's disease (AD) clinical trials. However, many amyloid positive (Am+) early-stage subjects do not worsen clinically during a clinical trial, and a neurodegenerative measure predictive of decline could provide critical information. Studies have shown correspondence between perfusion measured by early amyloid frames post-tracer injection and fluorodeoxyglucose (FDG) positron emission tomography (PET), but with limitations in sensitivity. Multivariate machine learning approaches may offer a more sensitive means for detection of disease related changes as we have demonstrated with FDG.

Methods: Using summed dynamic florbetapir image frames acquired during the first 6 minutes post-injection for 107 Alzheimer's Disease Neuroimaging Initiative subjects, we applied optimized machine learning to develop and test image classifiers aimed at measuring AD progression. Early frame amyloid (EFA) classification was compared to that of an independently developed FDG PET AD progression classifier by scoring the FDG scans of the same subjects at the same time point. Score distributions and correlation with clinical endpoints were compared to those obtained from FDG. Region of interest measures were compared between EFA and FDG to further understand discrimination performance.

Results: The EFA classifier produced a primary pattern similar to that of the FDG classifier whose expression correlated highly with the FDG pattern (R-squared 0.71), discriminated cognitively normal (NL) amyloid negative (Am–) subjects from all Am+ groups, and that correlated in Am+ subjects with Mini-Mental State Examination, Clinical Dementia Rating Sum of Boxes, and Alzheimer's Disease Assessment Scale–13-item Cognitive subscale (R = 0.59, 0.63, 0.73) and with subsequent 24-month changes in these measures (R = 0.67, 0.73, 0.50).

Discussion: Our results support the ability to use EFA with a multivariate machine learning–derived classifier to obtain a sensitive measure of AD-related loss in neuronal function that correlates with FDG PET in preclinical and early prodromal stages as well as in late mild cognitive impairment and dementia.

KEYWORDS
Alzheimer's disease, amyloid, early frame amyloid, EFA, fluorodeoxyglucose, machine learning

Highlights

- The summed initial post-injection minutes of florbetapir positron emission tomography correlate with fluorodeoxyglucose.
- A machine learning classifier enabled sensitive detection of early prodromal Alzheimer's disease.
- Early frame amyloid (EFA) classifier scores correlate with subsequent change in Mini-Mental State Examination, Clinical Dementia Rating Sum of Boxes, and Alzheimer's Disease Assessment Scale–13-item Cognitive subscale.
- EFA classifier effect sizes and clinical prediction outperformed region of interest standardized uptake value ratio.
- EFA classification may aid in stratifying patients to assess treatment effect.

1 | BACKGROUND

Dementia from Alzheimer's disease (AD) results in enormous economic and emotional burden for patients, caregivers, and health-care systems, mounting as the population ages. This has stimulated investment in development of therapeutic candidates to slow disease progression. However, in AD trials conducted over a 10-year period, 99.6% of trials failed to demonstrate efficacy, with only a single symptomatic treatment (memantine) approved during that period[1] and one new treatment, Aduhelm®, approved during the 10 years since. A weakness in many trials was the inaccuracy of clinical diagnosis. Amyloid positron emission tomography (PET) substudies in pivotal trials of two monoclonal antibodies targeting amyloid beta (Aβ) found many subjects enrolled using accepted clinical criteria for probable AD did not have significant brain amyloid burden.[2–4] As a result, screening with amyloid PET has been increasingly incorporated for subject inclusion.[5] However, even in amyloid-positive populations, clinical phenotypes and trajectories are highly variable. Identifying subjects with brain amyloid burden who are at greatest risk for decline could significantly increase the power to detect effects of treatments intended to slow progression and could inform decision making and when and to whom such treatments should be offered.

AD-related neurodegeneration correlates with clinical decline.[6] In preclinical AD, the presence of neurodegeneration has been proposed as a basis for disease staging.[7] Glucose hypometabolism measured with fluorodeoxyglucose (FDG) PET in amyloid-positive patients correlates with rates of cognitive decline in preclinical and later stages.[8] Decline in precuneus metabolism occurs 10 years before symptom onset in dominantly inherited AD, preceding hippocampal volume reductions by 5 years.[9,10] However, the need to reduce patient burden and the additional cost and radiation have led to the elimination of FDG PET as a biomarker in most clinical trials. Disease-related changes in blood flow parallel those in FDG PET as measured by [^{15}O]water PET,[11] [^{99m}Tc]-HMPAO single photon emission computed tomography,[12,13] and arterial spin labeling magnetic resonance imaging (MRI),[14] with differences apparent even in cognitively normal subjects at risk.[15,16] Blood flow measurement therefore represents a potential option for detecting neurodegeneration, of particular value in early stages during which cognitive and volumetric metrics may be less sensitive.[17,18]

The initial minutes post-injection of amyloid imaging have an established correlation with blood flow and have been explored as a possible approach to characterizing neurodegeneration without requiring an additional scan.[19–22] The basis is that the extraction rate from arterial plasma to tissue (K1 influx rate) of amyloid PET tracers such as Pittsburgh compound B ([^{11}C]-PiB[23]), [^{18}F]-florbetapir,[24] and [^{18}F]-florbetaben[25] correlates with cerebral blood flow.[19–21] This has been extended to a simplified measurement obtained by summing the first few amyloid frames post-tracer injection.[19] These early frames strongly correlate with FDG PET measures in cognitively normal (NL), mild cognitive impairment (MCI), and AD subjects.[20,26–28] However, differences in dynamic range have been noted, and early frame amyloid (EFA) has not shown significant differences between normal controls and the earliest stages of disease defined by amyloid status and clinical diagnosis.[25,29] Recently, discrimination between cognitively normal tau-negative versus tau-positive groups was demonstrated using EFA hippocampal values.[30]

We previously demonstrated that an optimized FDG PET multivariate image classifier can improve detection of AD-related neuronal

decline and prediction of subsequent clinical worsening in preclinical and prodromal AD.[31–34] In the present work, we evaluated the ability of an EFA classifier to provide a similar measure of neurodegeneration and to discriminate between cognitively normal amyloid-negative controls and early prodromal as well as later AD stages, and to predict rate of subsequent clinical decline. Using EFA data, we first developed and validated a classifier to measure the presence of an AD-like pattern. For comparison, we developed an FDG classifier using the FDG scans of the same subjects as available. To understand factors influencing performance, we evaluated the EFA scans directly using the FDG classifier and compared regional signal intensities in the EFA and FDG scans.

RESEARCH IN CONTEXT

1. **Systematic Review**: To support their analysis, the authors conducted a review of relevant literature using PubMed and abstracts and presentations available from conferences. Published findings regarding early frame amyloid (EFA) and its comparison to measures of blood flow and glucose metabolism, and extensions to early frame tau, have been appropriately cited.
2. **Interpretation**: The findings of this work build upon prior studies by demonstrating sensitivity of measures of brain blood flow as reflected by EFA positron emission tomography to progression of Alzheimer's disease (AD) using multivariate machine learning classifiers. These findings also illustrate robust relationships between quantitative scores for EFA pattern expression, fluorodeoxyglucose pattern expression, disease stage, and subsequent change in clinical endpoints.
3. **Future Directions**: Next steps are to demonstrate these relationships in a larger set of EFA data that is now available, evaluate longitudinal variability and statistical power, and further explore predictive relationships with subsequent clinical endpoint progression.

2 | METHODS

2.1 | Data

Data were obtained from the Alzheimer's Disease Neuroimaging Initiative (ADNI, adni.loni.usc.edu). The dynamic amyloid PET scans of 111 ADNI2 subjects imaged with florbetapir for 20 minutes immediately post-injection were downloaded in their unprocessed form (four 15-second, four 30-second, three 1-minute, three 2-minute, and two 4-minute frames). Scans were acquired using several different scanner models but a common acquisition protocol.

For comparison, we downloaded each subject's FDG PET scan acquired 30 to 60 minutes post-tracer injection from the same visit as available. Amyloid standardized uptake value ratio (SUVR) normalized to whole cerebellum and/or cerebrospinal fluid (CSF) Aβ42 levels were obtained to determine amyloid status. Visit-matched and 24-month follow-up Mini-Mental State Examination (MMSE), Clinical Dementia Rating Sum of Boxes (CDR-sb), and Alzheimer's Disease Assessment Scale–13-item Cognitive subscale (ADAS Cog-13) scores were obtained for clinical endpoint correlation.

2.2 | Image processing

Scans were inspected for image artifact and inter-frame subject motion. The discrete frames for each scan were aligned and co-registered to each participant's closest timepoint MRI. Spatial warping to a common template was performed using each subject's MRI and the VBM8 toolbox within SPM8,[35] and applying the transformation to the PET frames. To reconcile resolution across scanner models, an 8 mm Gaussian smoothing filter was applied.[36] Static images were generated by summing frames from the first 6 minutes of each scan,[26] and images were intensity normalized by z-scoring to whole brain without ventricles.

2.3 | Classifier development

In brief, "classifiers" in this work are image patterns that are visually interpretable and that optimize voxel intensities to maximize those that contribute to AD-related neurodegeneration, minimizing noise. For classifier development, we used the NPAIRS framework for machine learning[31,32,37] incorporated in our PipelineMax™ software to develop classifiers to quantify AD pattern expression.[33] In brief, N training classes are defined (in this case groups of images). NPAIRS uses principal component (PC) analysis to identify an uncorrelated set of intensity patterns that in combination account for the variance across the data set. Canonical variates analysis (CVA, a form of linear discriminant analysis) is used to mathematically combine selected PCs into a set of N-1 image intensity patterns (CVs) that discriminate classes. By taking relationships between regions into account, and segregating out "noise" components that would be embedded in a univariate analysis, the classifier can help increase statistical power. To avoid overfitting, NPAIRS splits the data set into two halves many times, each time developing a model from each half and generating metrics of reproducibility (correlation between the models for each half) and prediction (classification accuracy of each half by the other half). These are used to select parameters for a robust, generalizable consensus classifier. The model can then be used to evaluate (score) independent scans (with no need for inputting other information, and without the need to develop a new classifier for each study) by mathematically comparing the voxel intensities in the scan to the relevant CV and assigning a numeric score reflecting the degree to which the scan expresses the associated pattern of intensities.

Our initial EFA classifier was based upon 63 training subjects allocated to five classes defined based upon clinical diagnosis and amyloid

(Am; positive [+] or negative [−]) status: NL−,[10] SMC− (subjective memory complaint),[19] NL/SMC+,[11] MCI+ (5 early MCI [EMCI+], 5 late MCI [LMCI+]), AD+,[14] with consideration to balancing age and sex. These classes were defined to provide a representative spectrum of disease over which the classifier could identify progression pattern(s). Subjects were selected for training if they had clearly defined amyloid status including agreement between CSF Aβ and florbetapir SUVR values regarding amyloid positive/negative status, and for MCI and AD categories if they were amyloid positive. Positivity thresholds were florbetapir SUVR > 1.11[38] and a CSF Aβ value < 192.[39] CSF Aβ values between 192 and 209 or florbetapir SUVR values between 1.08 and 1.15 (14–27 centiloids [CL])[40] were considered a threshold zone and excluded from training due to variation in CSF Aβ cutoffs reported by ADNI and amyloid PET measurement variability. Am+ training subjects had SUVRs from 1.18 and 1.73 (33–136 CL). The classifier was validated using a leave-one-out (LOO) process in which NPAIRS was applied to 63 sets of 62 subjects with a stratified split-half across the classes. A normalized first canonical variate (CV1) pattern that accounted for the largest between-class variance of each of the 63 NPAIRS models was used to predict the CV score of each of the 63 LOO subjects. A consensus classifier pattern was determined based on a weighted average across the 63 models' CV1 patterns. For comparison, we developed an FDG PET classifier using the same subjects and class definitions, and the same approach described above. FDG scans were available for 56 of the 63 subjects.

The consensus EFA classifier, FDG classifier, and a FDG AD progression classifier previously developed in a similar manner with 133 training subjects[29] were applied to the remaining 48 subjects to further evaluate correlation between EFA and FDG classifier scores. Becauses these subjects had clinical diagnoses of MCI or AD but negative or threshold amyloid burden and did not meet training class criteria, they were not used for independent testing of classification accuracy. However, their scores were compared to those of Am+ subjects with the same clinical diagnoses to explore possible differentiation. EFA scans were also scored directly by the FDG classifier.

2.4 | Region of interest analysis

Mean signal intensities were measured in posterior cingulate, angular gyrus, and temporal regions that exhibit progressive hypometabolism in AD,[41] and other regions including anterior cingulate and occipital cortex. Regions in which metabolism is relatively preserved in AD, and that have been used as reference regions in FDG analyses[42] were evaluated including cerebellum, pons, and thalamus. A MetaROI (region of interest) consisting of the average of values in posterior cingulate, angular gyrus, and lateral (inferior and middle) temporal regions[41] was evaluated using three different reference regions: whole brain, cerebellar cortex, and pons. Probabilistic region masks were defined based upon Automated Anatomical Labeling (AAL)[43] boundaries, tailored to fit the gray matter within the spatial normalization template, and eroded by two voxels (three to four for pons and cerebellar cortex) to minimize spillover from adjacent tissue. Mean intensities were measured on spatially normalized images using PMOD v3.3 (PMOD Technologies).

2.5 | Statistical analyses

EFA classifier score effect sizes (ES) were compared to those generated for the same visit FDG scans by the FDG classifier and our previously developed FDG AD Progression classifier[33] (calculated using Hedge's g [(comparator group mean − control group mean)/(pooled, weighted standard deviation], with bias adjustment), to account for group sizes and differences in standard deviation between groups).[44] Age effects were assessed by regressing the EFA CV1 scores of NL−/SMC− subjects with age to determine whether a significant relationship was present. EFA and FDG ROI values were compared and percent deviation from whole brain calculated as an indicator of dynamic range. Relationships were explored between classifiers and between each imaging measure (EFA classifier scores, FDG classifier scores, EFA MetaROI SUVRs) and MMSE, CDR-sb, and ADAS-Cog 13 at time of scan as well as change over 24 months post-scan (Pearson's R). Significance was assessed using two-tailed *t*-tests; $P < .05$ was considered significant.

3 | RESULTS

3.1 | Subject characteristics and training selection

Characteristics of subjects whose EFA scans met quality control requirements are summarized in Table 1. In this data set, 26% of subjects diagnosed as AD, 55% of LMCI, 71% of EMCI, and 82% of NL subjects (with or without SMC) were Am− as measured using the amyloid PET SUVR. Of the 90 subjects having CSF values available, 21% had conflicting amyloid PET and CSF Aβ assignments or were in the "threshold zone" and not used for training.

3.2 | Classifier results

EFA classifier development resulted in a CV1 pattern of relative hypo- and hyper- (or preserved) perfusion that characterized the cross-sectional progression from NL− to AD+. Figure 1A shows the mean LOO test scores by class, while Figure 1B shows representative slices from the corresponding consensus CV1 pattern. Regions of declining activity (blue) included posterior cingulate, precuneus, parietotemporal cortices, medial temporal, and inferior lateral temporal regions, while motor cortex and cerebellum were hyper- (or preserved; red) in signal relative to whole brain. This pattern was similar to the FDG AD progression classifier and consistent with neurodegenerative patterns reported in the literature.[32,33,45] There was no difference between NL− and SMC−. In comparisons of NL/SMC− to other groups, ES and *P*-values were: NL/SMC+ ES 0.76 ($P < .023$), EMCI+ 0.94 ($P < .054$), LMCI+ 1.47 ($P < .004$), MCI+ combined ES 1.39 ($P < .0004$), and AD+ ES 3.40 ($P < .0000$; Figure 2B, 2 g.3).

TABLE 1 Subject characteristics

Dx	N	Age (years)	Sex (%F)	*APOE ε4* carrier	Educ (years)	MMSE	LDEL-TOT	CDR-sb	ADAS-Cog 13	Florbetapir SUVR	Aβ CSF
Subjects used in training and Leave-One-Out (LOO) validation											
NL−	10	77 (5.7)	40%	10%	16 (2.6)	29 (1.9)	15 (3.3)	0.1 (0.2)	9 (6.4)	1.00 (0.0)	249[16]
SMC−	19	74 (5.7)	63%	5%	17 (2.5)	29 (1.5)	14 (2.8)	0.2 (0.2)	8 (3.2)	1.01 (0.0)	242[24]
NL/SMC+	11	78 (5.6)	55%	55%	16 (3.0)	28 (1.1)	13 (4.1)	0.5 (0.6)	9 (3.0)	1.51 (0.2)	134[25]
EMCI+	4	75 (11.2)	50%	75%	14 (1.9)	29 (1.9)	12 (2.8)	1.4 (1.4)	13 (4.9)	1.42 (0.1)	143[16]
LMCI+	5	76 (8.9)	40%	100%	15 (4.9)	28 (1.8)	5 (2.4)	2.2 (1.2)	17 (6.1)	1.46 (0.1)	124[4]
AD+	14	74 (5.8)	50%	86%	15 (3.2)	23 (3.4)	1 (1.2)	4.6 (1.9)	30 (8.8)	1.48 (0.1)	119[21]
Additional subjects not included in training or LOO but scored using the classifier											
NL/SMC	22	75 (8.9)	41%	27%	17 (3.2)	29 (1.0)	14 (4.3)	0.1 (0.2)	9 (4.3)	1.08 (0.1)	195[39]
EMCI	13	73 (8.2)	38%	23%	17 (2.5)	29 (1.6)	12 (4.4)	1.3 (0.8)	9 (5.0)	1.08 (0.2)	209[30]
LMCI	8	76 (10.2)	50%	25%	17 (2.7)	28 (1.8)	7 (4.1)	1.4 (1.6)	12 (5.3)	1.00 (0.1)	202[37]
AD	5	79 (12.9)	20%	0%	17 (2.8)	22 (2.7)	2 (3.4)	5.7 (3.4)	26 (6.4)	0.98 (0.0)	233[23]

Note: Among the additional subjects who were not used in training were subjects whose amyloid status was at threshold or conflicted between amyloid PET and CSF Aβ values, and amyloid negative MCI and AD subjects. Values are mean (SD) except where percentages are given.

Abbreviations: Aβ, amyloid beta; AD, Alzheimer's disease; ADAS-Cog 13, Alzheimer's Disease Assessment Scale−13-item Cognitive subscale; *APOE*, apolipoprotein E; CDR-sb, Clinical Dementia Rating sum of boxes; CSF, cerebrospinal fluid; EMCI, early mild cognitive impairment; LDEL-TOT, logical memory delayed score; LMCI, late mild cognitive impairment; NL, Alzheimer's Disease Neuroimaging Initiative clinical diagnosis of cognitively normal; SMC, subjective memory complaint; SUVR, standardized uptake value ratio.

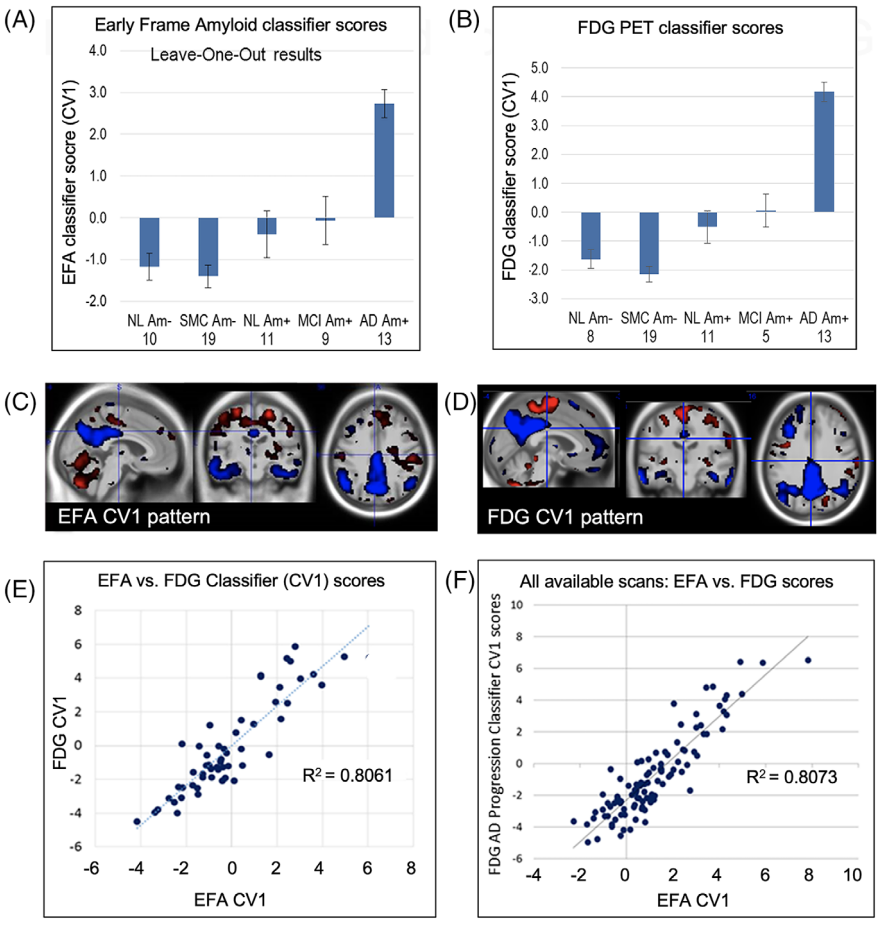

FIGURE 1 Mean CV1 scores (bars = SEM) by training group generated during independent LOO (A) EFA classifier scoring of summed first 6-minute scans, and (B) FDG classifier scoring of FDG scans for the same subjects and visit where available. Consensus CV1 pattern associated with the primary canonical variates for the (C) EFA and (D) FDG classifiers. Plots showing correlation between (E) EFA and FDG classifier scores, and (F) EFA classifier scores versus scores resulting from evaluation of all FDG scans in the data set (including subjects not used in training or LOO) using the previously developed FDG AD progression classifier. AD, Alzheimer's disease; CV1, first canonical variate; EFA, early frame amyloid; FDG, fluorodeoxyglucose; LOO, leave one out; MCI, mild cognitive impairment; NL, cognitively normal; SEM, standard error of the mean; SMC, subjective memory complaint

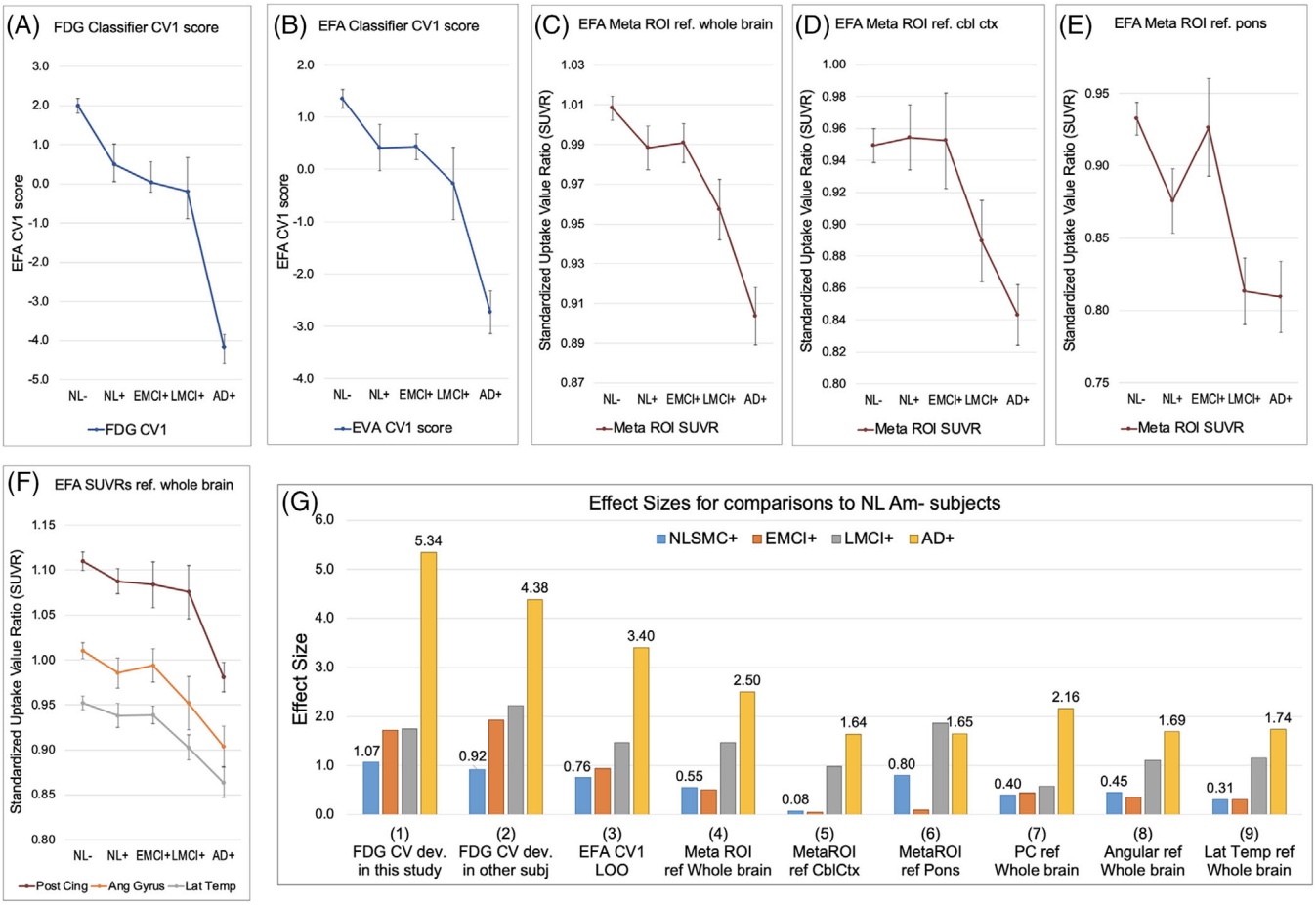

FIGURE 2 Mean values (with standard error of the mean bars) for NL/SMC−, NL+, EMCI+, LMCI+, and AD+ subjects for (A) FDG classifier developed using scans from this study; (B) EFA classifier; (C) EFA MetaROIs referenced to whole brain; (D) EFA MetaROIs referenced to cerebellar cortex; (E) EFA MetaROIs referenced to pons; (F) posterior cingulate, angular gyrus, and lateral temporal ROIs referenced to whole brain; and (G) comparison of effect sizes (ES) for[1] FDG classifier developed in this study,[2] FDG AD progression classifier developed using 133 subjects not in this study,[3] EFA classifier LOO results,[4,5,6] Meta ROI referenced to whole brain, cerebellar cortex, and pons, respectively,[7,8,9] posterior cingulate, angular gyrus, and lateral temporal ROIs referenced to whole brain. Labels show the ES values for NL+ and AD+ versus NL/SMC−. A complete listing is found in Table S1. AD, Alzheimer's disease; CV1, first canonical variate; EFA, early frame amyloid; EMCI, early mild cognitive impairment; ES, effect size; FDG, fluorodeoxyglucose; LOO, leave one out; LMCI, late mild cognitive impairment; MCI, mild cognitive impairment; NL, cognitively normal; ROI, region of interest; SEM, standard error of the mean; SMC, subjective memory complaint

The FDG classifier developed using FDG scans from the same subjects produced a similar primary CV1 pattern and mean scores (Figure 1C) for each class, despite unavailability of scans for seven subjects. The associated pattern (Figure 1D) showed relative hypo- and hypermetabolism similar to the EFA classifier and the previously developed FDG AD progression classifier. The difference between NL− and SMC− was not significant. Comparing NL/SMC− to other groups, ES and *P*-values were: NL/SMC+ ES 1.09, $P < .002$, EMCI+ ES 1.72 ($P < .0008$), LMCI+ ES 1.75 ($P < .0007$), MCI+ combined ES 2.04, $P < .0000$, and AD+ ES 5.34, $P < .0000$ (Figure 2 g.1). The greater ES of the FDG classifier is due to a larger dynamic range combined with lower variance. Results from applying the previously developed FDG classifier to FDG scans of this data set were: NL/SMC+ ES 0.92 ($P < .010$), EMCI+ ES 1.93 ($P < .0000$), LMCI+ ES 2.22 ($P < .0000$), and AD+ ES 4.38, $P < .0000$ (Figure 2 g.2).

EFA LOO CV1 scores correlate with FDG classifier CV1 scores for the same subjects ($N = 56$, $R = 0.90$, $P < .000$, Figure 1E). A comparison of EFA CV1 scores for all subjects having FDG PET scans available with the previously developed FDG AD progression classifier scores for those subjects produced similar correlation values ($N = 96$, $R = 0.90$, $P < .000$, Figure 1F). There was no correlation between EFA CV1 score and age within Am− NL or SMC subjects ($N = 29$, age 68–86 years, $R = 0.24$), and within Am+ NL or SMC subjects ($N = 33$, age 64–86 years, $R = 0.02$).

EFA CV1 scores for subjects not used in training were concordant with FDG scores. EFA CV1 scores for 17 NL or SMC subjects who were amyloid PET negative but CSF Aβ positive or threshold were similar to NL− scores (−1.39 +/- 0.85), while three subjects who were amyloid PET positive had slightly higher scores (−0.60 +/- 0.80). For 12 EMCI subjects who were amyloid PET negative but with mixed CSF Aβ status,

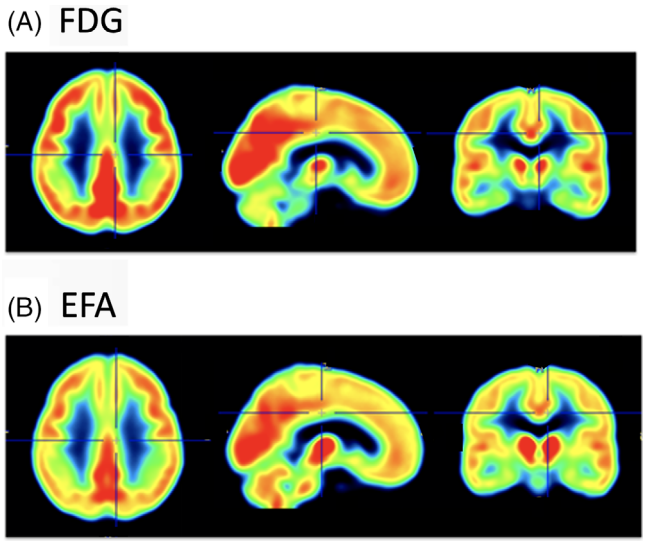

FIGURE 3 A, Mean fluorodeoxyglucose (FDG) image and (B) mean early frame amyloid (EFA) image representing the average of scans from cognitively normal Am− subjects, intensity normalized to whole brain

EFA CV1 averaged 0.21 +/-1.71 and was the most variable, while the amyloid PET positive EMCI subject was pattern positive (−0.15). For six LMCI subjects who were amyloid PET negative but with threshold or positive CSF Aβ values as available, EFA CV1 scores averaged −0.87 +/-0.80, resembling amyloid negative NL/SMC subjects. Of five amyloid negative subjects with a clinical diagnosis of AD, four scored as having CV scores in the range of the Am+ MCI or AD subjects, driven primarily by very low signal in temporal cortices. Two subjects exceeded thresholds for positivity in CSF total tau and/or phosphorylated tau (80 pg/ml and 39 pg/ml, respectively[39]) but two were below threshold.

When EFA scans were scored directly by the FDG AD progression classifier, NL− and SMC− subjects scored similarly to EMCI+ subjects, and the progression slope was greatly diminished until reaching later MCI and AD stages, where scoring of EFA and FDG scans approximately converged.

3.3 | Region of interest comparisons

Similar patterns, but different in dynamic range, were evident when comparing FDG and EFA images. As illustrated in Figure 3, cortical EFA signal tended to be lower and subcortical and cerebellar signal higher compared to FDG. Table 2 lists region of interest values normalized to whole brain within NL/SMC−, MCI+, and AD+ groups, comparing EFA and FDG. EFA signal in most cortical regions is lower than in FDG relative to whole brain, whereas EFA signal in typical reference regions and in limbic structures such as hippocampus is greater. This results in lower SUVR values in EFA overall, particularly in NL and EMCI+ subjects, and a reduced differential between NL− and stages of AD.

Comparisons of the posterior cingulate, angular gyrus, lateral temporal, and MetaROI SUVR effect sizes to those of the EFA and FDG classifiers are shown in Figure 2 and Table S1 in supporting information. EFA ROIs referenced to pons lacked a consistent trajectory toward AD+ until reaching LMCI+. EFA ROIs referenced to cerebellar cortex showed no discrimination between NL− and NL+ or EMCI+. EFA ROIs referenced to whole brain did not differ between NL− and NL+ or EMCI+ but differed between NL− versus LMCI+ and AD+.

3.4 | Comparisons to clinical endpoints

Within Am+ subjects, correlations were observed between EFA CV1 scores ($N = 35$) and MMSE ($R = 0.61$), CDR-sb ($R = 0.62$), and ADAS-Cog 13 ($R = 0.72$; Figure 4A,E), between FDG CV1 scores ($N = 29$) and MMSE ($R = 0.76$), CDR-sb ($R = 0.79$) and ADAS-Cog 13 (0.89; Figure 4B,E), and between EFA MetaROI SUVRs referenced to whole brain and MMSE ($R = 0.63$, $P <$), CDR-sb ($R = 0.64$), and ADAS-Cog 13 ($R = 0.77$). All P-values were <.0001.

Imaging measures showed significant relationships to the subsequent 24-month change in clinical endpoints as follows (Figure 4): EFA CV1 scores versus ΔMMSE ($N = 24$, $R = 0.67$, $P < .0003$), ΔCDR-sb ($N = 27$, $R = 0.73$, $P < .00002$), ΔADAS-Cog 13 ($N = 24$, $R = 0.50$, $P < .012$; Figure 4C,E); FDG CV1 scores versus ΔMMSE ($N = 19$, $R = 0.71$, $P < .0008$), ΔCDR-sb ($N = 22$, $R = 0.67$, $P < .0007$), ΔADAS-Cog 13 ($N = 19$, $R = 0.73$, $P < .0004$; Figure 4D,E); and MetaROIs referenced to whole brain versus ΔMMSE ($N = 24$, $R = 0.39$, $P < .057$ trend), ΔCDR-sb ($N = 27$, $R = .49$, $P < .009$), ΔADAS-Cog 13 ($N = 24$, $R = 0.73$, $P < .057$ trend; Figure S1 in supporting information). When evaluating EFA measures using only those subjects for whom FDG data were available, R-values remained very similar for ΔMMSE and ΔCDR-sb and increased for ΔADAS-Cog 13 (EFA CV1 $R = 0.59$, EFA MetaROIs $R = 0.47$; Figure 4E).

4 | DISCUSSION

In this exploratory work, we have shown that using a multivariate classifier developed with the early post-injection frames of florbetapir PET can be used to quantify expression of a pattern that is highly correlated with FDG PET across the AD progression spectrum. EFA classifier scores also showed strong correlation with both same-visit scores and subsequent clinical decline in MMSE and CDR-sb, suggesting the ability to identify patients who are most likely to worsen as we have previously demonstrated using FDG PET.[33] The EFA classifier showed superior performance in detecting early (NL+ and EMCI+) changes and predicting clinical decline compared to ROI approaches used in this study and in prior published work.[29]

The correlation between EFA and FDG is consistent with published research.[26,29,46] As in prior studies,[26,29,47] we found lower EFA signal in cortical regions and greater EFA signal in typically preserved subcortical structures. Differences between blood flow and metabolism, and a slower K2 efflux rate of the amyloid tracer, could contribute to this. The 28% difference in pons, for example, was equivalent to that found by Gur et al., who directly measured blood flow using O15

TABLE 2 Region of interest values relative to whole brain and differences between EFA and FDG

	FDG				EFA				Difference % (EFA-FDG)/FDG			
	NL−	NL+	MCI+	AD+	NL−	NL+	MCI+	AD+	NL−	NL+	MCI+	AD+
Middle frontal	1.23 (0.06)	1.20 (0.07)	1.17 (0.07)	1.15 (0.09)	1.11 (0.04)	1.13 (0.07)	1.09 (0.05)	1.11 (0.08)	−11	−6	−7	−3
Superior frontal	1.14 (0.06)	1.14 (0.06)	1.11 (0.07)	1.10 (0.09)	1.05 (0.04)	1.08 (0.07)	1.04 (0.04)	1.07 (0.09)	−9	−6	−7	−3
Posterior cingulate	1.27(0.05)	1.25 (0.06)	1.19 (0.03)	1.06 (0.08)	1.16 (0.06)	1.14 (0.05)	1.13 (0.03)	1.03 (0.07)	−9	−10	−6	−3
Angular gyrus	1.15 (0.08)	1.11 (0.08)	1.08 (0.04)	0.93 (0.12)	1.06 (0.07)	1.05 (0.07)	1.02 (0.09)	0.94 (0.09)	−9	−6	−6	1
Middle occipital	1.10 (0.08)	1.08 (0.07)	1.07 (0.06)	1.04 (0.11)	1.02 (0.07)	1.01 (0.07)	1.00 (0.11)	0.99 (0.06)	−8	−7	−7	−5
Inferior parietal	1.13 (0.06)	1.09 (0.08)	1.06 (0.01)	1.00 (0.12)	1.05 (0.05)	1.06 (0.06)	1.01 (0.05)	0.98 (0.09)	−7	−3	−5	−2
Inferior temporal	1.01 (0.05)	0.99 (0.08)	0.96 (0.04)	0.86 (0.08)	0.96 (0.06)	0.96 (0.07)	0.92 (0.06)	0.86 (0.08)	−5	−3	−4	0
Supplemental motor	1.11 (0.06)	1.14 (0.04)	1.13 (0.07)	1.19 (0.07)	1.07 (0.06)	1.13 (0.09)	1.11 (0.04)	1.16 (0.08)	−4	−1	−2	−3
Middle temporal	1.08 (0.07)	1.06 (0.08)	1.06 (0.03)	0.94 (0.08)	1.05 (0.07)	1.03 (0.07)	1.03 (0.05)	0.95 (0.08)	−4	−3	−3	1
Putamen	1.35 (0.08)	1.37 (0.11)	1.38 (0.08)	1.43 (0.11)	1.32 (0.06)	1.32 (0.07)	1.35 (0.08)	1.38 (0.09)	−2	−4	−3	−3
Superior temporal	1.07 (0.04)	1.04 (0.05)	1.06 (0.03)	1.03 (0.06)	1.07 (0.05)	1.04 (0.06)	1.06 (0.01)	1.02 (0.05)	0	0	0	−1
Anterior cingulate	1.06 (0.05)	1.06 (0.06)	1.05 (0.04)	1.06 (0.10)	1.08 (0.07)	1.06 (0.06)	1.08 (0.07)	1.10 (0.12)	2	1	4	4
Subcortical white	0.72 (0.03)	0.76 (0.05)	0.74 (0.02)	0.77 (0.05)	0.74 (0.05)	0.77 (0.04)	0.76 (0.03)	0.78 (0.06)	3	2	3	2
Cerebellar cortex	1.01 (0.05)	1.00 (0.05)	1.05 (0.08)	1.06 (0.05)	1.12 (0.07)	1.11 (0.06)	1.16 (0.07)	1.14 (0.07)	10	10	10	7
Hippocampus	0.79 (0.04)	0.78 (0.03)	0.77 (0.06)	0.74 (0.09)	0.89 (0.04)	0.87 (0.05)	0.86 (0.08)	0.80 (0.08)	11	10	10	7
Amygdala	0.80 (0.05)	0.79 (0.02)	0.79 (0.06)	0.75 (0.09)	0.92 (0.05)	0.90 (0.04)	0.90 (0.04)	0.83 (0.08)	13	13	12	10
Thalamus	1.07 (0.06)	1.05 (0.08)	1.07 (0.08)	1.08 (0.11)	1.27 (0.05)	1.24 (0.04)	1.26 (0.09)	1.25 (0.13)	15	15	15	14
Pons	0.82 (0.05)	0.87 (0.06)	0.89 (0.05)	0.89 (0.06)	1.13 (0.06)	1.19 (0.09)	1.17 (0.12)	1.18 (0.10)	28	27	24	25

Abbreviations: AD, Alzheimer's disease; EFA, early frame amyloid; FDG, fluorodeoxyglucose; MCI, mild cognitive impairment; NL, cognitively normal.

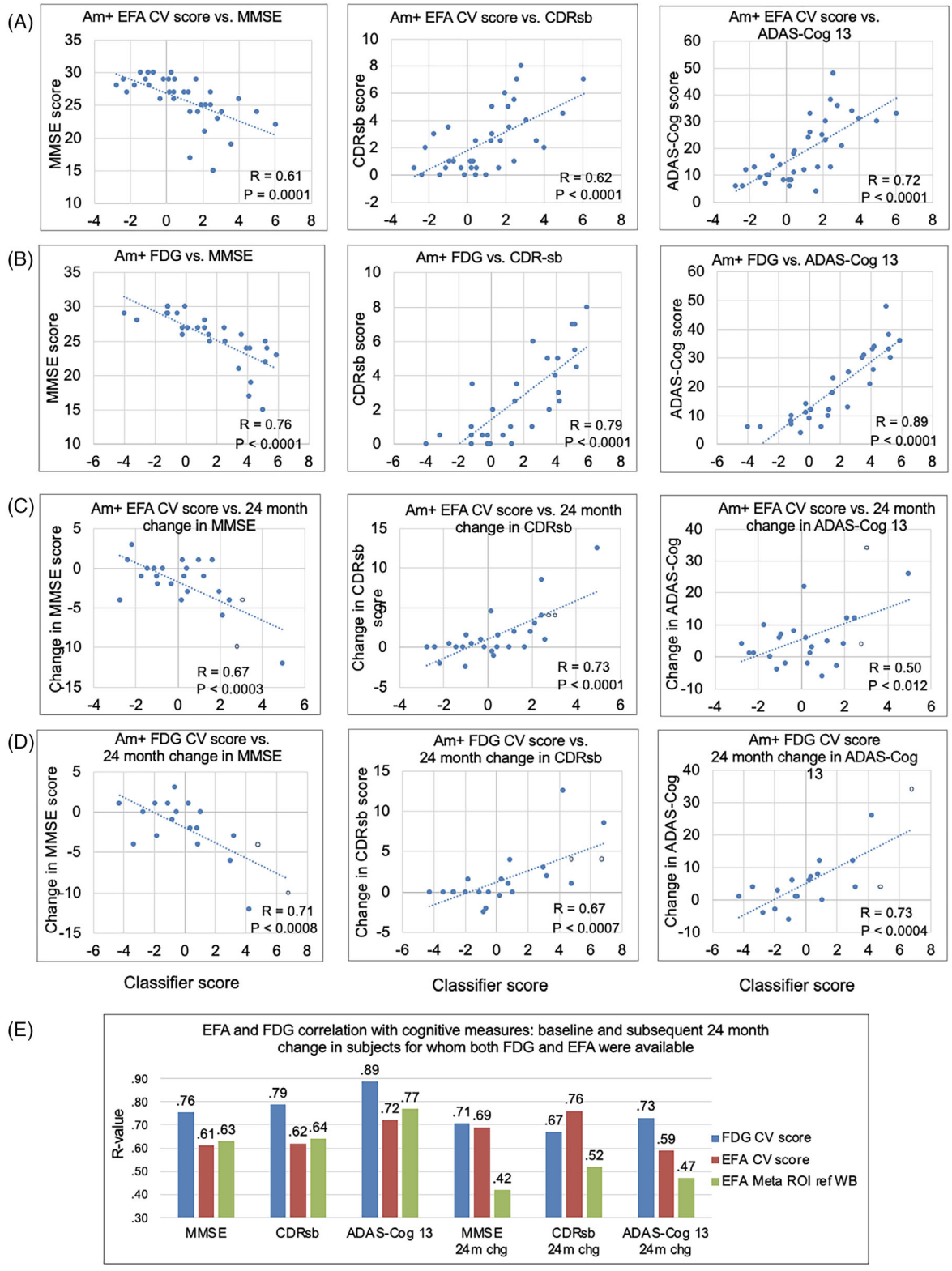

FIGURE 4 Correlation between (A) EFA classifier scores and (B) FDG classifier scores with MMSE, CDR- sb, and ADAS-Cog 13 scores at the same visit time point as the scan; (C) EFA classifier scores and (D) FDG classifier scores with the change in MMSE, CDR-sb, and ADAS-Cog 13 scores over the 24 months after the scan. The two unfilled circles in each case are the subjects where only 12-month follow-up was available and the slope applied to estimate a 24-month change. E, Comparison of Pearson's *R*-values for the FDG classifier, EFA classifier, and EFA MetaROI referenced to whole brain, using only those subjects who had both EFA and FDG PET scans available. Bar labels are *R*-values. ADAS-Cog 13, Alzheimer's Disease Assessment Scale–13-item Cognitive subscale; CDR-sb, Clinical Dementia Rating sum of boxes; CV, canonical variate; EFA, early frame amyloid; EMCI, early mild cognitive impairment; ES, effect size; FDG, fluorodeoxyglucose; LOO, leave one out; LMCI, late mild cognitive impairment; MCI, mild cognitive impairment; MMSE, Mini-Mental State Examination; NL, cognitively normal; PET, positron emission tomography; ROI, region of interest

PET.[47] In either case, the net effect is to reduce the dynamic range of the signal that is relevant to detection of preclinical and prodromal AD using standard ROI methods.[26,29] Comparison among ROI methods demonstrated the criticality of reference region, potentially related to differences described here.

Previous studies using imaging endpoints to detect neurodegeneration in clinically healthy elderly as a contributor to cognitive decline have often used a MetaROI for FDG PET,[41] brain atrophy by MRI, or a combination.[8,48,49] Studies of EFA as a potential surrogate for FDG PET have also used ROI approaches and have not demonstrated discrimination from cognitively normal Am– subjects until reaching LMCI,[29] consistent with ROI findings in this data set. An important aspect of our work is that we have addressed limitations in sensitivity encountered when applying standard ROI measurement to EFA to detect preclinical and early prodromal AD.[26,29] The hippocampus, reported to discriminate tau-positive versus negative cognitively normal subjects,[26] is a prominent feature of the classifier pattern although other regions in the pattern (e.g., posterior cingulate, precuneus) likely aid in discriminating AD versus non-AD states, staging disease, and predicting likely decline. EFA data could be particularly important for preclinical populations, in which neurodegeneration is a key element of staging guidelines[7] and given evidence that amyloid positivity combined with neurodegeneration is associated with greater subsequent decline.[8]

In differentiating progressive disease stages, the FDG classifier ES exceeded those of EFA (57% greater for NL– vs. AD+); however, EFA classifier correlation to subsequent change in clinical endpoints was nearly identical to FDG for ΔMMSE and exceeded FDG for ΔCDR-sb given the same subjects. Superior FDG performance may be offset by the burden of adding an extra scan.

Of note in this data set were the relatively high proportions of Am– AD and MCI subjects and the number of subjects whose amyloid burden was near threshold, or with disagreement between CSF Aβ values and florbetapir PET SUVR. The uncertainty of amyloid status close to threshold suggests the further benefit of characterizing subjects with regard to an AD-specific neurodegeneration pattern. In the AD+ stage, the classifier did not always discriminate between Am+ and Am–. This is due to overlapping regional effects between different dementias, but differentiation can be achieved[46] using an additional classification step as we and others have previously demonstrated with FDG PET.[33]

Limitations in this study were the number and range of subjects with conclusive Am+ burden available for classifier development. This constrained the ability to rigorously evaluate classifier performance over different stages and in predicting subsequent clinical decline. The data were cross sectional only. A longitudinal EFA study of florbetapir and florbetaben PET scans was added to ADNI3, which should provide information on signal variability over time[50] and a larger number of subjects for classifier development and validation. Conditions for subjects during the uptake period for an amyloid PET scan differ from the standards used during FDG PET scans, and whether standardization of conditions would improve predictive value remains to be determined. Target-related binding emerging in the latter part of early frames could argue for using R1 values derived from the two-phase data instead. R1 values for [^{11}C]-PiB have been reported to have higher test–retest reliability for longitudinal studies[22] and greater sensitivity to disease severity[51] and can be used in kinetic modeling to dissociate blood flow effects from amyloid.[48]

The logistics of acquiring EFA scans must be considered for this approach to be routinely implemented in clinical trials. Imaging a patient immediately post-tracer injection requires additional scanner time as well as staff time and training related to acquisition, reconstruction, storage, and transfer of the additional frames, as they are separated in time from the amyloid burden acquisition. The need to initiate image acquisition just after injection introduces complexity but can be addressed with brief assistance by a second person who needs only to activate the control to start the scan upon cue from the PET technologist.

While EFA is not proposed here to determine patient inclusion/exclusion, our findings suggest that it could provide a powerful additional tool to determine which patients are at greatest risk for clinical decline, to better assess treatment effect in these patients. By using optimized classification methods, this benefit becomes feasible in preclinical and early prodromal stages during which identification of neurodegenerative progression may be most critical.

ACKNOWLEDGMENTS

Data collection and sharing for the ADNI comparator subjects used in this project was funded by the Alzheimer's Disease Neuroimaging Initiative (ADNI; National Institutes of Health Grant U01 AG024904) and DOD ADNI (Department of Defense award number W81XWH-12-2-0012). ADNI is funded by the National Institute on Aging, the National Institute of Biomedical Imaging and Bioengineering, and through generous contributions from the following: AbbVie; Alzheimer's Association; Alzheimer's Drug Discovery Foundation; Araclon Biotech; BioClinica, Inc.; Biogen; Bristol-Myers Squibb Company; CereSpir, Inc.; Eisai Inc.; Elan Pharmaceuticals, Inc.; Eli Lilly and Company; EuroImmun; F. Hoffmann-La Roche Ltd and its affiliated company Genentech, Inc.; Fujirebio; GE Healthcare; IXICO Ltd.; Janssen Alzheimer Immunotherapy Research & Development, LLC; Johnson & Johnson Pharmaceutical Research & Development LLC; Lumosity; Lundbeck; Merck & Co., Inc.; Meso Scale Diagnostics, LLC; NeuroRx Research; Neurotrack Technologies; Novartis Pharmaceuticals Corporation; Pfizer Inc.; Piramal Imaging; Servier; Takeda Pharmaceutical Company; and Transition Therapeutics. The Canadian Institutes of Health Research is providing funds to support ADNI clinical sites in Canada. Private sector contributions are facilitated by the Foundation for the National Institutes of Health (www.fnih.org). The grantee organization is the Northern California Institute for Research and Education, and the study has been coordinated by the Alzheimer's Disease Cooperative Study at the University of California, San Diego. ADNI data are disseminated by the Laboratory for Neuro Imaging at the University of Southern California. This work was supported in part by Janssen Research and Development. The development of the AD Progression Classifier by ADM Diagnostics was previously funded in part by SBIR grant award IIP-1256638 from the National Science Foundation.

CONFLICTS OF INTEREST

Dawn C. Matthews, Ana S. Lukic, and Randolph D. Andrews are employees of ADM Diagnostics, Inc., a company that provides imaging clinical trial services and diagnostic products. Stephen C. Strother and Miles N. Wernick are senior advisors to ADM Diagnostics, Inc. Mark E. Schmidt is an employee of Janssen Pharmaceutica, NV. None of these authors have a conflict of interest regarding use of florbetapir as an amyloid PET tracer. Author disclosures are available in the supporting information.

AUTHOR CONTRIBUTIONS

Dawn C. Matthews was responsible for analysis design, a portion of analyses, and manuscript writing. Ana S. Lukic performed the classifier development using software jointly designed and developed in consultation with Stephen C. Strother and Miles N. Wernick, and all three provided manuscript review and editing. Randolph D. Andrews performed image data quality control and processing and provided manuscript input. Mark E. Schmidt provided study direction and participated in manuscript writing and review. Data used in the preparation of this article were obtained from the Alzheimer's Disease Neuroimaging Initiative (ADNI) database (adni.loni.usc.edu).

REFERENCES

1. Cummings JL, Morstorf T, Zhong K. Alzheimer's disease drug-development pipeline: few candidates, frequent failures. *Alzheimers Res Ther*. 2014;6(4):37.
2. Salloway S, Sperling R, Fox NC, et al. Two phase 3 trials of bapineuzumab in mild-to-moderate Alzheimer's disease. *N Engl J Med*. 2014;370(4):322-333.
3. Siemers ER, Sundell KL, Carlson C, et al. Phase 3 solanezumab trials: secondary outcomes in mild Alzheimer's disease patients. *Alzheimers Dement*. 2016;12(2):110-120.
4. Liu E, Schmidt ME, Margolin R, et al. Amyloid-beta 11C-PiB-PET imaging results from 2 randomized bapineuzumab phase 3 AD trials. *Neurology*. 2015;85(8):692-700.
5. Sevigny J, Suhy J, Chiao P, et al. Amyloid PET screening for enrichment of early-stage Alzheimer disease clinical trials: experience in a phase 1b clinical trial. *Alzheimer Dis Assoc Disord*. 2016;30(1):1-7.
6. Ewers M, Brendel M, Rizk-Jackson A, et al. Reduced FDG-PET brain metabolism and executive function predict clinical progression in elderly healthy subjects. *Neuroimage Clin*. 2014;4:45-52.
7. Sperling RA, Aisen PS, Beckett LA, et al. Toward defining the preclinical stages of Alzheimer's disease: recommendations from the National Institute on Aging-Alzheimer's Association workgroups on diagnostic guidelines for Alzheimer's disease. *Alzheimers Dement*. 2011;7(3):280-292.
8. Mormino EC, Betensky RA, Hedden T, et al. Synergistic effect of beta-amyloid and neurodegeneration on cognitive decline in clinically normal individuals. *JAMA Neurol*. 2014;71(11):1379-1385.
9. Bateman RJ, Xiong C, Benzinger TL, et al. Clinical and biomarker changes in dominantly inherited Alzheimer's disease. *N Engl J Med*. 2012;367(9):795-804.
10. Jack CR, Knopman DS, Jagust WJ, et al. Tracking pathophysiological processes in Alzheimer's disease: an updated hypothetical model of dynamic biomarkers. *Lancet Neurol*. 2013;12(2):207-216.
11. Ishii K, Sasaki M, Matsui M, et al. A diagnostic method for suspected Alzheimer's disease using H(2)15O positron emission tomography perfusion Z score. *Neuroradiology*. 2000;42(11):787-794.
12. Bartenstein P, Minoshima S, Hirsch C, et al. Quantitative assessment of cerebral blood flow in patients with Alzheimer's disease by SPECT. *J Nucl Med*. 1997;38(7):1095-1101.
13. Nihashi T, Yatsuya H, Hayasaka K, et al. Direct comparison study between FDG-PET and IMP-SPECT for diagnosing Alzheimer's disease using 3D-SSP analysis in the same patients. *Radiat Med*. 2007;25(6):255-262.
14. Wang Z, Das SR, Xie SX, et al. Arterial spin labeled MRI in prodromal Alzheimer's disease: a multi-site study. *Neuroimage Clin*. 2013;2:630-636.
15. Thambisetty M, Beason-Held L, An Y, Kraut MA, Resnick SM. APOE epsilon4 genotype and longitudinal changes in cerebral blood flow in normal aging. *Arch Neurol*. 2010;67(1):93-98.
16. Wierenga CE, Clark LR, Dev SI, et al. Interaction of age and APOE genotype on cerebral blood flow at rest. *J Alzheimers Dis*. 2013;34(4):921-935.
17. Wierenga CE, Hays CC, Zlatar ZZ. Cerebral blood flow measured by arterial spin labeling MRI as a preclinical marker of Alzheimer's disease. *J Alzheimers Dis*. 2014;42(Suppl 4):S411-9.
18. Hays CC, Zlatar ZZ, Wierenga CE. The utility of cerebral blood flow as a biomarker of preclinical Alzheimer's disease. *Cell Mol Neurobiol*. 2016;36(2):167-179.
19. Meyer PT, Hellwig S, Amtage F, et al. Dual-biomarker imaging of regional cerebral amyloid load and neuronal activity in dementia with PET and 11C-labeled Pittsburgh compound B. *J Nucl Med*. 2011;52(3):393-400.
20. Forsberg A, Engler H, Blomquist G, Langstrom B, Nordberg A. The use of PIB-PET as a dual pathological and functional biomarker in AD. *Biochim Biophys Acta*. 2012;1822(3):380-385.
21. Chen YJ, Rosario BL, Mowrey W, et al. Relative 11C-PiB delivery as a proxy of relative CBF: quantitative evaluation using single-session 15O-water and 11C-PiB PET. *J Nucl Med*. 2015;56(8):1199-1205.
22. Bilgel M, Beason-Held L, An Y, Zhou Y, Wong DF, Resnick SM. Longitudinal evaluation of surrogates of regional cerebral blood flow computed from dynamic amyloid PET imaging. *J Cereb Blood Flow Metab*. 2020;40(2):288-297.
23. Klunk WE, Engler H, Nordberg A, et al. Imaging brain amyloid in Alzheimer's disease with Pittsburgh Compound-B. *Ann Neurol*. 2004;55(3):306-319.
24. Lister-James J, Pontecorvo MJ, Clark C, et al. Florbetapir f-18: a histopathologically validated Beta-amyloid positron emission tomography imaging agent. *Semin Nucl Med*. 2011;41(4):300-304.
25. Yoon HJ, Kim BS, Jeong JH, et al. Dual-phase (18)F-florbetaben PET provides cerebral perfusion proxy along with beta-amyloid burden in Alzheimer's disease. *Neuroimage Clin*. 2021;31:102773.
26. Hsiao IT, Huang CC, Hsieh CJ, et al. Correlation of early-phase 18F-florbetapir (AV-45/Amyvid) PET images to FDG images: preliminary studies. *Eur J Nucl Med Mol Imaging*. 2012;39(4):613-620.
27. Daerr S, Brendel M, Zach C, et al. Evaluation of early-phase [(18)F]-florbetaben PET acquisition in clinical routine cases. *Neuroimage Clin*. 2017;14:77-86.
28. Myoraku A, Klein G, Landau S, Tosun D. Alzheimer's Disease Neuroimaging I. Regional uptakes from early-frame amyloid PET and (18)F-FDG PET scans are comparable independent of disease state. *Eur J Hybrid Imaging*. 2022;6(1):2.
29. Lin KJ, Hsiao IT, Hsu JL, et al. Imaging characteristic of dual-phase (18)F-florbetapir (AV-45/Amyvid) PET for the concomitant detection of perfusion deficits and beta-amyloid deposition in Alzheimer's disease and mild cognitive impairment. *Eur J Nucl Med Mol Imaging*. 2016;43(7):1304-1314.
30. Raman F, Fang YD, Grandhi S, et al. Dynamic amyloid PET: relationships to flortaucipir Tau PET measures. *J Nucl Med*. 2021;63(2):287-293.
31. Strother SC, Anderson J, Hansen LK, et al. The quantitative evaluation of functional neuroimaging experiments: the NPAIRS data analysis framework. *Neuroimage*. 2002;15(4):747-771.
32. Strother SCMD, Lukic A, Andrews R, Wernick M. Superior Performance of a Multi-Stage PET Classifier for the Alzheimer's Disease

Cascade. Organization of Human Brain Mapping Annual Meeting; Quebec, Canada 2011.
33. Matthews DC, Lukic AS, Andrews RD, et al. Dissociation of down syndrome and Alzheimer's disease effects with imaging. *Alzheimers Dement (N Y)*. 2016;2(2):69-81.
34. Matthews DC, Andrews RD, Marendic B, Yokoyama M, Lukic AS, Alzheimer's Disease Neuroimaging Initiative. Neurodegenerative variability among amyloid positive MCI patients: Implications for clinical trials and clinical care. Alzheimer's Association International Conference (AAIC); Washington, D.C.: Alzheimer's Association; 2015.
35. Ashburner J. A fast diffeomorphic image registration algorithm. *Neuroimage*. 2007;38(1):95-113.
36. Joshi A, Koeppe RA, Fessler JA. Reducing between scanner differences in multi-center PET studies. *Neuroimage*. 2009;46(1):154-159.
37. Strother SOA, Spring R, Grady C, editor The NPAIRS Computational Statistics Framework for Data Analysis in Neuroimaging. Proceedings of COMPSTAT'2010; 2010: Physica-Verlag HD.
38. Landau SM, Thomas BA, Thurfjell L, et al. Amyloid PET imaging in Alzheimer's disease: a comparison of three radiotracers. *Eur J Nucl Med Mol Imaging*. 2014;41(7):1398-1407.
39. Shaw LM, Vanderstichele H, Knapik-Czajka M, et al. Cerebrospinal fluid biomarker signature in Alzheimer's disease neuroimaging initiative subjects. *Ann Neurol*. 2009;65(4):403-413.
40. Royse SK, Minhas DS, Lopresti BJ, et al. Validation of amyloid PET positivity thresholds in centiloids: a multisite PET study approach. *Alzheimers Res Ther*. 2021;13(1):99.
41. Landau SM, Harvey D, Madison CM, et al. Associations between cognitive, functional, and FDG-PET measures of decline in AD and MCI. *Neurobiol Aging*. 2011;32(7):1207-1218.
42. Minoshima S, Frey KA, Foster NL, Kuhl DE. Preserved pontine glucose metabolism in Alzheimer disease: a reference region for functional brain image (PET) analysis. *J Comput Assist Tomogr*. 1995;19(4):541-547.
43. Tzourio-Mazoyer N, Landeau B, Papathanassiou D, et al. Automated anatomical labeling of activations in SPM using a macroscopic anatomical parcellation of the MNI MRI single-subject brain. *Neuroimage*. 2002;15(1):273-89. doi:10.1006/nimg.2001.0978
44. Hedges LV. Distribution theory for Glass' estimator of effect size and related estimators. *J Educ Stat*. 1981;6(2):107-128. doi:10.3102/10769986006002107
45. Herholz K, Nordberg A, Salmon E, et al. Impairment of neocortical metabolism predicts progression in Alzheimer's disease. *Dement Geriatr Cogn Disord*. 1999;10(6):494-504.
46. Rostomian AH, Madison C, Rabinovici GD, Jagust WJ. Early 11C-PIB frames and 18F-FDG PET measures are comparable: a study validated in a cohort of AD and FTLD patients. *J Nucl Med*. 2011;52(2):173-179.
47. Gur RC, Ragland JD, Reivich M, Greenberg JH, Alavi A, Gur RE. Regional differences in the coupling between resting cerebral blood flow and metabolism may indicate action preparedness as a default state. *Cereb Cortex*. 2009;19(2):375-382.
48. Jack CR, Jr, Wiste HJ, Weigand SD, et al. Different definitions of neurodegeneration produce similar amyloid/neurodegeneration biomarker group findings. *Brain*. 2015;138(Pt 12):3747-3759.
49. Bilgel M, An Y, Helphrey J, et al. Effects of amyloid pathology and neurodegeneration on cognitive change in cognitively normal adults. *Brain*. 2018;141(8):2475-2485.
50. Health FftNIo. Alzheimer's Disease Neuroimaging Initiative 3 (ADNI 3) 2021 [Program overview including early frame amyloid PET add-on study]. Available from: https://www.fnih.org/our-programs/alzheimers-disease-neuroimaging-initiative-3-adni-3
51. Ottoy J, Verhaeghe J, Niemantsverdriet E, et al. (18)F-FDG PET, the early phases and the delivery rate of (18)F-AV45 PET as proxies of cerebral blood flow in Alzheimer's disease: validation against (15)O-H2O PET. *Alzheimers Dement*. 2019;15(9):1172-1182.

SUPPORTING INFORMATION

Additional supporting information can be found online in the Supporting Information section at the end of this article.

How to cite this article: Matthews DC, Lukic AS, Andrews RD, et al. Measurement of neurodegeneration using a multivariate early frame amyloid PET classifier. *Alzheimer's Dement*. 2022;8:e12325. https://doi.org/10.1002/trc2.12325